Available online at www.sciencedirect.com
SCIENCE DIRECT
Polymer 46 (2005) 2579–2583
polymer
www.elsevier.com/locate/polymer

Visualisation of the structure transfer between an oriented polymer melt and the semi-crystalline state

Norbert Stribeck[a,*], Rüdiger Bayer[b], Peter Bösecke[c], Armando Almendarez Camarillo[a]

[a]*Institut für Technische und Makromolekulare Chemie, Universität Hamburg, Bundesstrasse 45, 20146 Hamburg, Germany*
[b]*Institut für Werkstofftechnik, Universität GH Kassel, Mönchebergstrasse 3, 34125 Kassel, Germany*
[c]*ESRF, 6 rue Jules Horowitz, B.P. 220, 38043 Grenoble Cedex 9, France*

Received 9 July 2004; received in revised form 4 November 2004; accepted 25 January 2005

Abstract

Structure evolution of highly oriented polyethylene during cautious melting and crystallization is investigated with both high time resolution and high signal-to-noise ratio by means of small-angle X-ray scattering (SAXS) and wide-angle X-ray scattering (WAXS). The two-dimensional SAXS patterns are transformed to the multidimensional chord distribution function (CDF) in physical space. The results are continuous and smooth movies of the nanostructure, which elucidate the mechanisms of the evolution of semicrystalline structure.

We find that in our material crystallization is preceeded by a rather diffuse mesomorphic nanostructure. Based on its variation in relation to other observed features like row nuclei and crystalline lamellae, we propose to associate it to phase separated regions of entangled and disentangled chain segments, respectively. The movies show that the mesophase structure holds the key for the understanding of crystallite orientation and arrangement in the fibre.

Keywords: Crystallization; Nanostructure; SAXS

1. Introduction

The understanding of polymer crystallization is central for the tailoring of materials properties and again is in the scientific discussion [1–7]. Nevertheless, the views concerning the evolution of the corresponding semicrystalline nanostructure are still conflicting, because the experimental data collected so far are still incomplete. In this paper, we report first results of a method that appears apt to narrow the mentioned gap and is resting on both in situ experiments with high time resolution using oriented materials, and on an advanced technique of data analysis.

By means of imaging methods like atomic force microscopy (AFM) or scanning near-field optical microscopy (SNOM) it appears very difficult to in situ monitor a structure transfer process executed under technical conditions with sufficient resolution corresponding to both time and space [8–10]. Utilising X-ray scattering, such experiments are possible, but the recorded data require mathematical evaluation, as long as it is not considered to apply simplified notions. Many papers have been published during the last two decades that report on investigations in which X-ray patterns are collected with a high time resolution aiming at a 'peak position analysis'. For this task images with a typical maximum count of 200 have been reported in many studies. Because of the poor counting statistics [11] of such measurements the corresponding data are insufficient for a quantitative analysis of either peak shape or Fourier analysis.

If, today, we combine sufficiently equipped synchrotron radiation facilities with an advanced Fourier analysis concept for the investigation of oriented polymer materials, we are enabled to study the processes of structure transfer in two or three dimensions of physical space. Recently, we have already reported results based on corresponding crystallization experiments [12–14], which have been carried out with a time resolution of 2 min at the Hamburg Synchrotron Laboratory (HASYLAB), where this exposure time is the minimum to guarantee sufficient data quality.

* Corresponding author. Tel.: +49 40 42838 3615; fax: +49 40 42838 6008.
E-mail address: norbert.stribeck@desy.de (N. Stribeck).

0032-3861/$ - see front matter © 2005 Published by Elsevier Ltd.
doi:10.1016/j.polymer.2005.01.076

Because of the coarse time pattern some basic questions concerning the mechanisms of melting and crystallization remained unanswered. We found, for example, row structure nuclei before the first lamellae showed up; two minutes later there was nothing but a crowd of oriented lamellae placed at random positions. We postulated that the statistical placement should have been preceded by a regular and long ranging 'shish kebab' [15] structure. Here we present first results from extended series of similar experiments that have been recorded at the European Synchrotron Radiation Facility (ESRF) in Grenoble with a good signal-to-noise ratio and a time resolution of 7 s. Utilising such a fine time pattern with scattering patterns qualified for Fourier analysis we are entering a new field of continuous and multidimensional investigation of nanostructure evolution, and thus achieve new vistas concerning the mechanisms that are governing the processing of polymer materials.

In order to record such data streams, a powerful X-ray source and two modern two-dimensional (2D) detectors are required. The concept of scattering pattern analysis developed by us utilises methods of image processing that have successfully been applied in medical technology for years. Combined we obtain a detailed image in physical space of the correlations among the surfaces of nanosize domains in the material. This image is the multidimensional chord distribution function (CDF) [16–18].

2. Experimental section

2.1. Material and setup

Polyethylene samples (Lupolen 6021 D, BASF, thickness: 2 mm) from high-pressure injection moulded [19] rods are molten and crystallized in the synchrotron beam of beam line ID02 at the ESRF in Grenoble. Data are recorded using two 2D detectors. In the critical regions of the temperature profile the cycle time between consecutive snapshots is set to 7 s. USAXS images are collected by a two-dimensional position sensitive XRII-FReLoN ('Fast Readout, Low Noise') CCD detector developed at ESRF (driven in 1024×1024 pixel mode of each $0.164\times0.164\ \mathrm{mm}^2$, 14 bit resolution). The sample-to-detector distance is set to 10 m. Wide-angle X-ray scattering (WAXS) is simultaneously recorded using a MCP-Sensicam CCD detector positioned [20,21] at a short distance of the sample.

USAXS exposure is dynamically adapted during the experiment between 0.1 and 3 s in order to always use the full linear range of the detector, i.e. in every image the most intense valid pixel is exposed to about 14,000 counts. The primary beam is attenuated by a factor of 10 in order to keep the exposure in a reasonable range with respect to the accuracy of available timers and counters. A minimum cycle time of 7 s between two snapshots provides for both control of exposure and data storage (4 s) of single snapshots. We use to start with an exposure of 0.3 s as soon as the material is reaching a temperature of 120 °C, then decrease it to 0.1 s up to the moment when most of the material is melting. Thereafter, we instantly increase to 3 s and finally slowly adjust to lower exposure.

2.2. Data analysis

Data analysis is carried out with computer programs developed under Linux and pv-wave [22] in order to extract information on nanostructure (i.e. a topology $\rho(\mathbf{r})\in[\rho_{\mathrm{cryst}}, \rho_{\mathrm{amorph}}]$ of phases with distinct densities) from two-dimensional (2D) SAXS patterns. The result is an 'edge-enhanced autocorrelation function' $z(\mathbf{r})$—the autocorrelation of the gradient field $\nabla\rho(\mathbf{r})$. Thus as a function of ghost displacement, $\mathbf{r}$, the CDF $z(\mathbf{r})$ shows peaks where ever there are domain surface contacts between domains in $\rho(\mathbf{r})$ and in its displaced ghost. The CDF with fibre symmetry in real space, $z(r_{12}, r_3)$, is computed from the fibre-symmetric SAXS pattern, $I(s_{12}, s_3)$, of multi-phase materials with uniaxial orientation [16]. No model is required to compute the CDF. Apart from uniaxial symmetry we only assume that the nanostructure is sufficiently imperfect. In the historical context, the CDF is an extension of Ruland's interface distribution function (IDF) [23] to the multi-dimensional case or, in a different view, the Laplacian of Vonk's multidimensional correlation function [24].

Spot testing and interpretation of individual snapshots from the large series of data turned out to be error-prone. In order to become able to describe the principal phases of the process, perception was improved by combining four patterns (small-angle X-ray scattering (SAXS), wide-angle X-ray scattering (WAXS) and the CDF from two different view points) in one picture frame and, finally, by concatenating the frames into a movie. For this purpose, the free computer programs PoVRay, ImageMagick, transcode and mplayer were utilised. In the running movie the phases of nanostructure evolution become clear, and we can pick representative frames for the purpose of demonstration and an aspired quantitative analysis.

3. Results and discussion

The movies that show the nanostructure evolution in real space are available for download on the web (http://www.chemie.uni-hamburg.de/tmc/stribeck/crys/).

Fig. 1 shows one movie frame from the beginning of the crystallization containing combined measurement data (Fig. 1(a)–(d)) and a sketch of the corresponding nanostructure (Fig. 1(e)). The CDF (c, d) displays the correlations among domain surfaces in the nanostructure for displacements of 300 nm in two directions (fibre direction r_3 and transverse direction r_{12}, respectively). Fibre direction is indicated by an arrow in the base plane of the three-dimensional (3D) plots.

In the cooling melt, we do not only observe the becoming

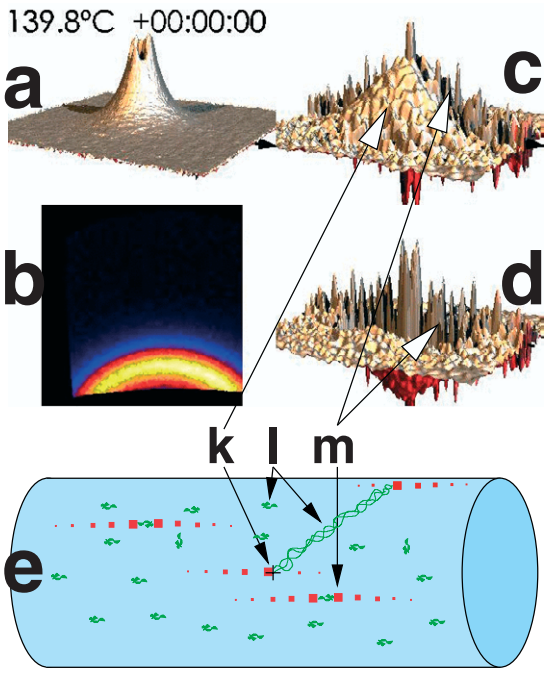

Fig. 1. Structure of the oriented polyethylene melt. (a–d) Four views of the measured data are combined in one movie frame. (a) SAXS, (b) WAXS, (c) CDF (top view), (d) CDF (bottom view). Fibre axis in (b) vertical, otherwise horizontal. (e) Sketch of the nanostructure.

and passing of crystal nuclei which form row structures along the fibre axis [25] (Fig. 1, m). In addition, a broad pyramid-shaped elevation (Fig. 1, k) shows up in the CDF. According to the mathematical design of the CDF it characterises correlations between opposite surfaces of some kind of domains. Because of the broad monotonous character of the pyramid peak at this stage of the crystallization, the shapes of the corresponding domains are poorly defined. The movies show that these domains appear together with row nuclei on the meridian of the CDF. Thus we decided to call them 'row nuclei associated domains' (RADs). The reason that we dare to address the RADs 'domains' is both in their subsequent evolution before the first crystals are observed, and, at the time when crystallization is starting, in the observed correlations between its distinct features and the developing semicrystalline structure. This evolution indicates that the RADs may be identified by strands in the polymer chain network, in which chain entanglements are accumulated (Fig. 1, l), the nuclei being located at the tips of these domains. By strands of different length and orientation such a structure is initially diffuse but governing a considerable, nevertheless finite volume in the neighbourhood of a deliberate nucleus (Fig. 1, k). The size of this volume is given by the extension of the pyramid shaped structure observed in the CDF. In the sketch below the movie frame (Fig. 1, e) it is indicated by a cylindrical envelope.

Upon increasing temperature of the melt we observe, how the material is loosing its memory [26]: the volume controlled by the RADs is shrinking, and when finally the correlations of nuclei with each other are no longer restricted to the fibre direction, the material has lost most of its orientation memory, as the chain entanglements have become randomly distributed in the melt.

Let us study a melt, the orientation memory of which is still fairly well preserved. Upon decreasing temperature we observe that the monotonous distribution of distances between the tips of the RADs is developing into distinct maxima which move outward in correlation space (Fig. 2, n) before any crystallization is observed. At this stage, for the first time a domain structure is undoubtedly observed. We interpret the observed transition as a mesophase separation process causing the merging of single entanglements and RADs into more compact RADs of preferential size and orientation. The CDF maxima are not found on the meridian (fibre axis). Thus the most probable RAD is becoming an entangled strand that is extending in an inclined direction with respect to the fibre direction.

Let us continue to watch crystallization and restrict our demonstration to the case of isothermal crystallization at 130 °C (highest crystallization temperature from our experimental series). In this case, the different mechanisms are most clearly separated from each other. In the beginning of crystallization in the top view of the CDF (Fig. 2, p) peaks from the first crystallites are showing up on the meridian, exactly between two RAD peaks. Thus, their average thickness is similar to the average extension of the RADs in fibre direction (24 nm). Their lateral extension cannot be read from the extension of the central peak, because it is veiled by the strong RAD peaks. Nevertheless, in the bottom view of the CDF we observe on the equator an extended self

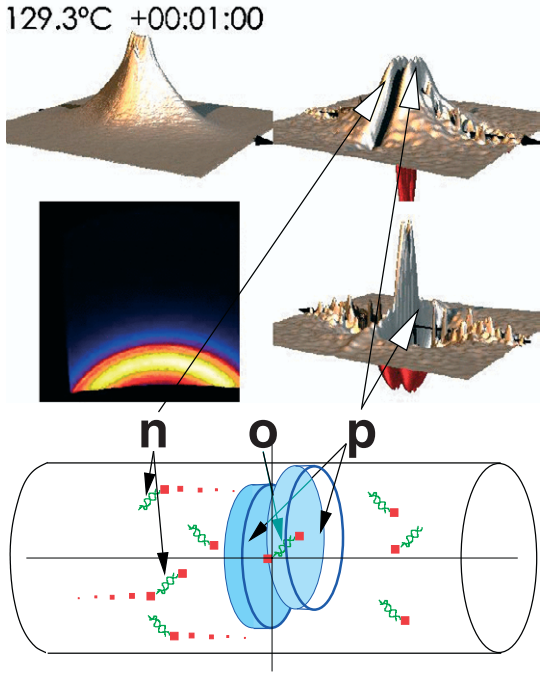

Fig. 2. Primary lamellae have formed.

correlation triangle that is a typical feature of lamellar systems [16]. Continuous growth of the base of this triangle exhibits that most of the lamellae are continuously growing. Nevertheless, a weak component from blocks arranged in planes [2] may be present. Although, the SAXS exhibits a high orientation, the orientation showing up in the WAXS pattern (pseudo colour image in Fig. 2) is low.

As crystallization is proceeding, the RADs are not substituted by an uncorrelated semicrystalline nanostructure in which the sizes of crystalline and amorphous domains are decoupled from the sizes of the RADs. Instead, the RAD peaks themselves are gradually compressed in fibre direction and converted into narrow and offset layer thickness peaks describing amorphous gaps between neighbouring lamellae. A similar but reverse process is observed during the melting of the original material. Thus, crystallization appears to be accompanied by a peculiar mesomorphic phase structure, which we associate to the network [1,27] of the entangled chains in the melt.

Based on these findings we propose a mechanism for the primary crystallization. According to it, the extension of the most probable RADs in fibre direction and the lateral shift of their tips is controlling, the primary lamellar structure. If a RAD is nucleating crystallites at *both* of its ends (Fig. 2, o), then its tips become the centres of two surfaces of offset neighbouring lamellae that are facing each other. In between is the amorphous layer with the entanglement-rich RAD. The inclination of the entangled strands that join two neighboured lamellae implies a component of lateral orientation of the corresponding amorphous region, as has been postulated by one of us in a model of crystallization from a melt that is containing multi-functional knots of entangled strands of chain molecules [27].

In the following 20 min we observe that both meridional peaks visible in the top view of the CDF (Fig. 3, small arrows) are moving in outward direction. Thus the average thickness of the crystalline layers is growing, but the distance between twin lamellae is almost kept constant. Thickness growth is oriented: away from the entanglement-rich RAD. During this phase, the observed orientation of the WAXS reflections is increasing, as is the number of lamellae during this phase. After about 20 min this statistical placement process [12–14] of single and twin layers comes to an end.

During the final stage of crystallization (Fig. 4) the broad triangular peaks in the top view of the CDF are split into a series of narrow peaks, the strength of which is strongly decreasing as a function of distance from the meridian. This CDF feature is expected for an ensemble of separated blocks that are placed in a plane (Strobl [2]). Even a little bit earlier and on the meridian, strong but narrow correlation peaks start to grow, showing that along fibre direction the emerging blocks are placed in such a way that they correlate strongly with each other. Anisotropy of the WAXS is lost during this phase, demonstrating that the blocky secondary crystals are not oriented.

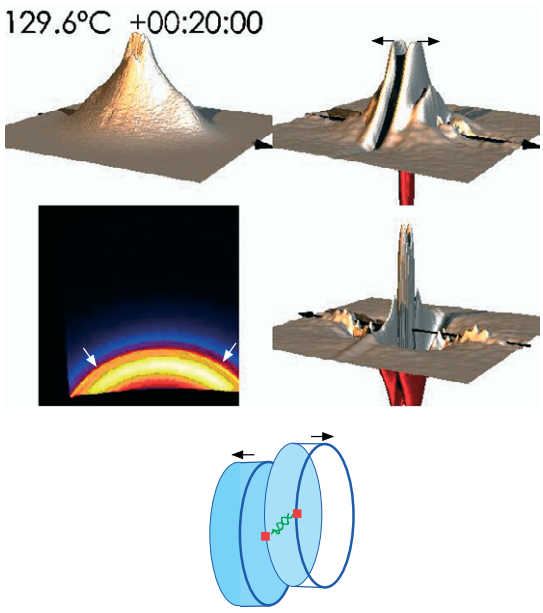

Fig. 3. Thickness growth (black arrows) of lamellae has finished. Maximum orientation (white arrows) in the WAXS.

In principle, our material passes through these phases even if the temperature profile is varied, but composition and size distributions of lamellae and blocks vary considerably. For example a narrow size distribution of secondary crystals (blocks) can be achieved by quenching from a high crystallization temperature. Nevertheless, in all our experiments carried out under ambient pressure the ultimate nanostructure is governed by the above-mentioned short-ranging networks of ‘frustrated’ crystal blocks. A

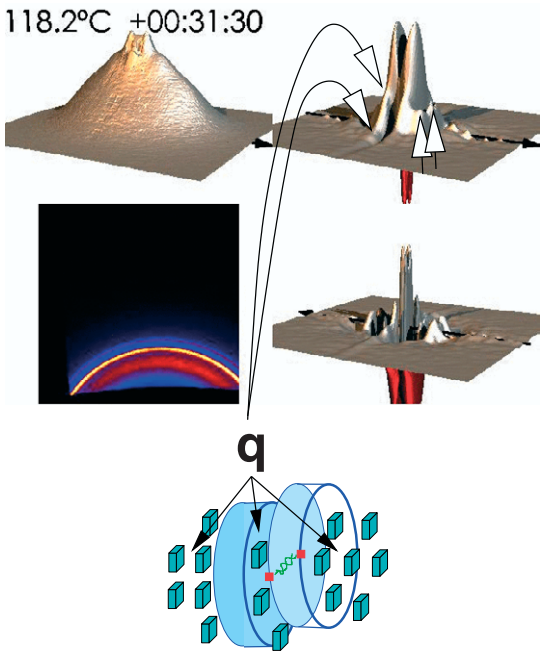

Fig. 4. Swarms of block-shaped secondary crystals are formed (q). The WAXS becomes isotropic.

mechanism similar to the two-step process (first extended oriented lamellae, then imperfect blocky crystallites) of polymer crystallization observed in situ by us has earlier been proposed on the basis of transmission electron microscopic studies [28–30].

It postulates that during growth front propagation at first 'dominant lamellae' are formed, which are followed by imperfect crystallites in 'subsidiary lamellae'.

4. Conclusions

Our in situ melting and crystallization experiments clearly show the evolution of the ensemble of crystalline domains and of the correlations among them. The method developed by us appears apt to elucidate the nanostructure evolution during processing and service of oriented polymer materials, in general. The only pre-requisition is that the process to be investigated can be carried out at a synchrotron beam line equipped with modern detectors and in situ control of the exposure. After the evaluation software is adapted to the actual set-up, the complete processing beginning from the recorded scattering pattern up to the combined 3D view of the nanostructure is carried out automatically. It must be stressed that this non-optimised straight-forward implementation of automated data evaluation, visualisation and sequence concatenation yields movies that are quite smooth. We expect that artificial variations still observable in the structure at low temperature can easily be eliminated, if also in this interval of the experiment the cycle time between two real snapshots is shortened. This is, of course, a matter of both data storage and computing capacity.

Nevertheless, we are still far from a desirable on-line visualisation of nanostructure on a time-scale of 1 s during the experiment that would provide the experimenter with in situ feedback. Presently we are able to transform 300 scattering patterns per hour to physical space, and the scene rendering of a movie takes another 10 h. Thus, in order to realise in situ feedback, computing power has to be raised by two orders of magnitude, not considered the present bottleneck of data readout.

A quantitative evaluation of the full set of crystallization experiments is reported in a follow-up paper [31].

Acknowledgements

We thank the European Synchrotron Radiation Facility, Grenoble, for beam time granted in the frame of project SC 1396.

References

[1] Heck B, Hugel T, Iijima M, Sadiku E, Strobl G. New J Phys 1999;1:171–1729.
[2] Heck B, Hugel T, Iijima M, Strobl G. Polymer 2000;41(25):8839–48.
[3] Heeley EL, Maidens AV, Olmsted PD, Bras W, Dolbnya IP, Fairclough JPA, et al. Macromolecules 2003;36(10):3656–65.
[4] Bras W, Dolbnya I, Detollenaere D, van Tol R, Malfois M, Greaves G, et al. J Appl Cryst 2003;36(3):791–4.
[5] Somani RH, Yang L, Hsiao BH, Fruitwala H. J Macromol Sci, Part B Phys 2003;B42(3):515–31.
[6] Somani RH, Yang L, Hsiao BS, Agarwal PK, Fruitwala HA, Tsou AH. Macromolecules 2002;35(24):9096–104.
[7] Yamazaki S, Hikosaka M, Toda A, Wataoka I, Yamada K, Tagashira K. J Macromol Sci, Part B Phys 2003;B42(3–4):499–514.
[8] Pearce R, Vancso GJ. Polymer 1998;39(5):1237–42.
[9] Hobbs JK, Humphris ADL, Miles MJ. Macromolecules 2001;34(16):5508–19.
[10] Humphris ADL, Hobbs JK, Miles MJ. Appl Phys Lett 2003;83(1):6–8.
[11] Klug HP, Alexander LE. X-ray diffraction procedures for polycrystalline and amorphous materials. 2nd ed. New York: Wiley; 1974.
[12] Stribeck N, Almendarez Camarillo A, Cunis S, Bayer RK, Gehrke R. Macromol Chem Phys 2004;205(11):1445–54.
[13] Stribeck N. Macromol Chem Phys 2004;205(11):1455–62.
[14] Stribeck N, Almendarez Camarillo A, Bayer R. Macromol Chem Phys 2004;205(11):1463–70.
[15] Barham PJ, Keller A. J Mater Sci 1985;20(7):2281–302.
[16] Stribeck N. J Appl Cryst 2001;34(4):496–503.
[17] Stribeck N, Buzdugan E, Ghioca P, Serban S, Gehrke R. Macromol Chem Phys 2002;203(4):636–44.
[18] Stribeck N, Funari SS. J Polym Sci, Part B Polym Phys 2003;41(16):1947–54.
[19] Stribeck N, Bayer R, von Krosigk G, Gehrke R. Polymer 2002;43(13):3779–84.
[20] Bösecke P, Diat O. J Appl Cryst 1997;30(5):867–71.
[21] Urban V, Panine P, Ponchut C, Bösecke P, Narayanan T. J Appl Cryst 2001;36(3):809–11.
[22] pv-wave. Version 7.5, Visual Numerics Inc., Boulder, Colorado; 2001.
[23] Ruland W. Colloid Polym Sci 1977;255(5):417–27.
[24] Vonk CG. Colloid Polym Sci 1979;257:1021–32.
[25] Keller A, Machin MJ. J Macromol Sci Phys 1967;B1(1):41–91.
[26] Khanna YP, Kumar R, Reimschuessel AC. Polym Eng Sci 1988;28(24):1607–11.
[27] Bayer RK. Colloid Polym Sci 1994;272(8):910–32.
[28] Bassett DC, Patel D. Polymer 1994;35(9):1855–62.
[29] Monks AW, White HM, Bassett DC. Polymer 1996;37(26):5933–6.
[30] Janimak JJ, Bassett DC. Polymer 1999;40(2):459–68.
[31] Stribeck N, Bösecke P, Bayer R, Almendarez Camarillo A. Progr Coll Polym Sci 2005; in press.